Pflügers Arch (1994) 427:399–405

Pflügers Archiv
European Journal of Physiology

Kinetic mode switch of rat brain IIA Na channels in *Xenopus* oocytes excised macropatches

Andrea Fleig[1,*], **Peter C. Ruben**[2], **Martin D. Rayner**[1]

[1] Department of Physiology, John A. Burns School of Medicine, University of Hawaii, Honolulu, HI 96822, USA
[2] Békésy Laboratory of Neurobiology, University of Hawaii, Honolulu, HI 96822, USA

Received September 6, 1993/Received after revision January 11, 1994/Accepted January 14, 1994

Abstract. Na currents recorded from inside-out macropatches excised from *Xenopus* oocytes expressing the α subunit of the rat brain Na channel IIA show at least two distinguishable components in their inactivation time course, with time constants differing about tenfold (τ_{h1} = approx. 150 µs and τ_{h2} = approx. 2 ms). In excised patches, the inactivation properties of Na currents changed with time, favoring the faster inactivation kinetics. Analysis of the fast and slow current kinetics shows that only the relative magnitudes of τ_{h1} and τ_{h2} components are altered without significant changes in the time constants of activation or inactivation. In addition, voltage dependence of both activation and steady-state inactivation of Na currents are shifted to more negative potentials in patches with predominantly fast inactivation, although reversal potentials and valences remained unaltered. We conclude that the two inactivation modes discerned in this study are conferred by two states of Na channel the interconversion of which are regulated by an as yet unknown mechanism that seems to involve cytosolic factors.

Key words: Sodium channel – Oocyte – Patch clamp

Introduction

Na channels are voltage-gated transmembrane proteins responsible for the propagation of electrically encoded signals in neurons, heart and skeletal muscle cells. In native membranes, Na channel properties have been studied in detail using the voltage-clamp method in different arrangements, such as axial wire, two-electrode voltage clamp (TEV), and patch clamp. The results of this work allow for the current concept of three functional states that the channel can occupy: closed, activated and inactivated. Typical gating behavior of macroscopic Na current upon depolarizing voltage steps reflects the successive transition of voltage- and state-dependent conformational changes in the protein. Voltage sensitivity and time course of transitions vary with the preparation, but typically both activation and inactivation are nearly complete within a few milliseconds. In some cells channel inactivation was found to be much delayed, yielding a slow decay of macroscopic Na currents [6, 23, 24]. To explain this phenomenon it has been suggested that the Na channel may adopt different gating modes. Furthermore, modulation of inactivation can be induced experimentally by diverse agents [2, 33, 36], excising the channels from the cellular environment [11, 18], or enzymatic regulation by kinases [22].

Advances in molecular biological techniques have made it possible to purify the Na channel protein and deduce its nucleic acid sequence [3, 9, 14, 19, 20, 27, 28, 30, 35]. In rat brain Na channels I, II, III and IIA the α subunit, a glycoprotein of 260 kDa co-purifies with two β subunits of 36 kDa and 33 kDa. The individual α subunits alone are sufficient to yield voltage-dependent currents when expressed in heterologous systems [3, 21, 34, 35]. Measured in *Xenopus* oocytes with TEV or cell-attached macropatch techniques the channels show unusually slow inactivation rates as compared to channels induced by injection with poly (A+) rat brain mRNA [4], or co-expression of the α and β1 subunits [7, 25]. However, channel gating in Chinese hamster ovary (CHO) cells expressing only the α subunit is comparable to native channel behavior under whole-cell conditions [31, 37].

We investigated macroscopic Na currents in excised macropatches of the inside-out configuration from *Xenopus* oocytes expressing rat brain IIA (RBIIA) Na channels. Under cell-free conditions we observe a unidirectional and time-dependent transition in channel inactivation from slow to predominantly fast kinetics, caused by a change in the equilibrium between at least two distinguishable gating modes. The fast inactivation rates in

* *Present address:* Max-Planck-Institute for Biophysical Chemistry, Department of Membrane Biophysics, Am Fassberg, D-37077 Göttingen, Germany
Correspondence to: A. Fleig

excised macropatches compare to channel behavior in native systems. Thus the unusually slow inactivation found in TEV experiments and cell-attached macropatches may be due, in part, to modulatory effects of the oocyte system on Na channels.

Materials and methods

Expression of mRNA in Xenopus oocytes. Full-length Na channel cDNA (pVA2580) linearized with *Cla* 1 served as the template for standard in vitro transcription with T7 RNA polymerase A (Promega) to generate functional mRNA. Oocytes for mRNA injection were obtained from laboratory-reared female *Xenopus laevis* (Nasco Biologicals) anesthetized in 0.1% tricaine methanesulfonate (Sigma) for aseptic removal of small portions of the ovaries. To isolate the cells and remove the follicular layer, oocytes were enzymatically treated by bathing them for 1–2 h in Ca^{2+}-free oocyte Ringer (OR-2) containing (in mM): NaCl 82.5, KCl 2, $MgCl_1$ 1, 4-(2-hydroxyethyl)-1-piperazineethanesulfonic acid (HEPES) 5, pH 7.5, with 2 mg/ml collagenase (Boehringer Mannheim) added. Individual oocytes were injected with mRNA using an automatic nanoinjector (Drummond Scientific).

Electrophysiological measurements. After 4–7 days of incubation at 16°C the oocytes were tested for expression using TEV clamp (Dagan). Na channel expression was high enough for macropatch recording between days 4 and 7 after microinjection of RBIIA mRNA. Oocytes with at least a 2 μA whole-cell current were selected for patch-clamp recording following removal of their vitelline membrane after exposure to a hyperosmotic solution containing (in mM): K-glutamate 200, KCl 20, $MgCl_2$ ethylenebis(oxonitrilo)tetraacetate (EGTA) 10, HEPES 10, pH 7.4. Patch electrodes (aluminosilicate, Sutter Instruments) were pulled in five stages, fire-polished and coated with Sylgard. The pipette solution (ND96) contained (in mM): NaCl 96, KCl 4, $CaCl_2$ 1.8, $MgCl_2$ 1, HEPES 5, pH 7.4. The bath solution (ISOP) contained (in mM): NaCl 9.6, KCl 88, $CaCl_2$ 1, $MgCl_2$ 1, EGTA 11, HEPES 5, pH 7.4.

Experimental methods and analysis. All experiments were conducted at room temperature (20–24°C). Recordings were made with an EPC-9 patch-clamp amplifier controlled by an ITC-16 interface (Instrutech) and a Macintosh Quadra 750 computer running Pulse and PulseFit software (HEKA) for data acquisition and analysis. Kinetic analysis and graphing was done with IGOR software (WaveMetrics).

All data shown are from three oocytes from two separate injection batches. Two to four patches that could be analyzed were obtained from each oocyte. All data records were acquired by averaging four sweeps and low-pass filtered at a cutoff frequency of 11.3 kHz. The number n refers to patches, unless indicated otherwise. Statistical evaluation was done using the Student's t-test. Current/voltage [I(V)] relationships were fitted by the product of a linear term and a Boltzmann function according to the equation:

$$g_{max} \cdot (V_m - E_{Na}) \cdot [1/1 + \exp^{-z(V_m - V_{1/2})/kT}]$$

where g_{max} is the maximal conductance, V_m the test potential, E_{Na} the reversal potential, z the valence, $V_{1/2}$ the voltage at half-maximal activation, k the Boltzmann constant, and T the absolute temperature. Steady-state activation and inactivation data were approximated by a Boltzmann function according to the equation:

$$1/1 + \exp^{-z(V_m - V_{1/2})/kT}.$$

The sum of three exponential functions describing the rising phase and the bi-phasic current decay were fitted to current traces to determine time constants (τ) and the intercepts of the functions

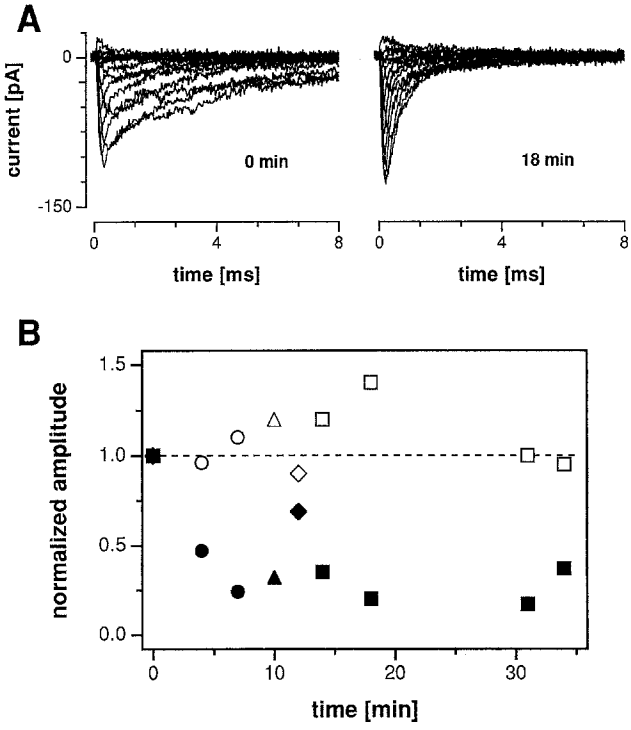

Fig. 1 A, B. Time dependence of the modal transition in excised patches. (A) Currents from oocytes injected with unitary rat brain IIA (RBIIA) Na channel mRNA at time zero (*left panel*) and 18 min after patch excision (*right panel*). Time zero designates the first current family acquired immediately after patch excision. A single test pulse to 0 mV preceded each first protocol to check for currents in the patch, but the first $I(V)$ measurements were rarely given later than 30 s after patch excision. Holding potential was −100 mV. A conditioning prepulse to −150 mV for 200 ms preceded a 10-ms test pulse to remove slow inactivation. Test potentials ranged from −60 mV to +60 mV (*left panel*) and from −80 mV to +60 mV (*right panel*). Test pulse frequency was 0.5 Hz. A P/4 procedure was applied to subtract linear leak and capacitive transient currents from the raw data. **B** Each data point represents the peak amplitude of fast (*open symbols*) and slow (*filled symbols*) currents at a test potential of −10 mV, corresponding symbols represent data from one patch. Amplitudes for fast mode were taken from the measured peak current amplitudes (I_{max}) corrected for background current. The amplitudes for the slow component were derived from tri-exponential fits. All amplitudes in a given patch were then normalized relative to the respective amplitude determined immediately after patch excision

at $t = 0$ for activation (A_a) and inactivation (A_{h1}, A_{h2}) according to the function:

$$(A_a \cdot \exp^{-t/\tau_a}) + (A_{h1} \cdot \exp^{-t/\tau_{h1}}) + (A_{h2} \cdot \exp^{-t/\tau_{h2}}) + A_{offset}$$

where t is time, and A_{offset} the baseline.

Results

Patch excision induces transition from slow to fast gating kinetics

Figure 1 A illustrates a typical example of kinetic alterations in Na currents recorded from inside-out macropatches excised from *Xenopus* oocytes expressing the α subunit of RBIIA. Initially, immediately after patch excision, families of Na currents evoked by depolarizing

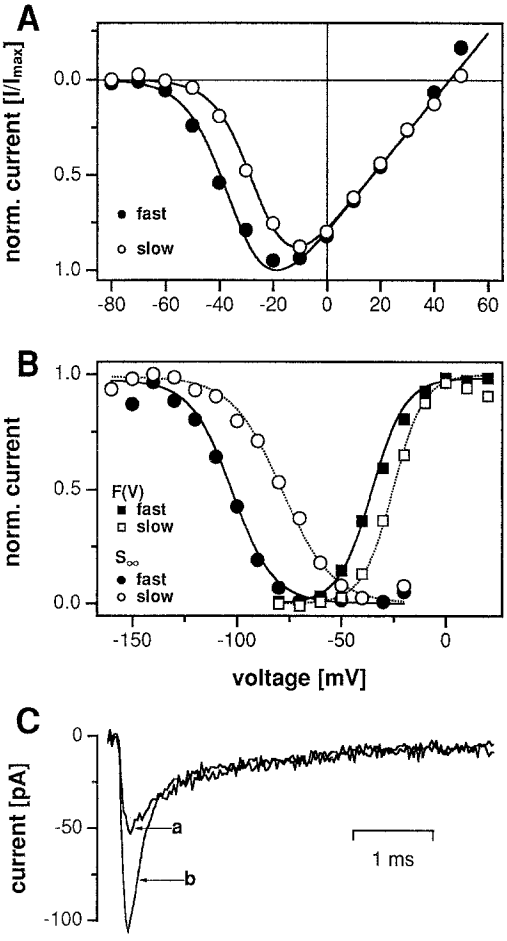

Fig. 2 A–C. Voltage dependence of activation and steady-state inactivation. *A* Normalized mean peak amplitudes (I/I_{max}) are plotted against test potential with corresponding mean $I(V)$ fits of fast (●) and slow (○) modes ($n = 5$ and $n = 7$, respectively). The mean amplitude ratios A_{h2}/I_{max} for the analyzed patches were 0.18 ± 0.1 for fast mode and 0.95 ± 0.1 for slow mode. The channels activate half-maximally at $V_{1/2(f)} = -33.8 \pm 3.3$ mV (mean ± SD, $n = 5$) and $V_{1/2(s)} = -24.8 \pm 2.3$ mV (mean ± SD, $n = 7$, $P < 0.005$). Valences z differ slightly with 97% certainty where $z_f = 3.2$ and $z_s = 3.5$. **B** Data represent the mean peak amplitudes of fast mode (●, ■) and slow mode (○, □), as indicated in the graph. $F(V)$ data were determined from peak amplitudes (i. e. normalized for maximal conductance and expressed as a fraction of open channels) and plotted as a function of variable test pulses (mV) preceded by a constant conditioning prepulse of −150 mV (duration: 200 ms). Half-maximal open probabilities of channels are $V_{1/2(f)} = -35.4 \pm 7$ mV (mean ± SD, $n = 5$) and $V_{1/2(s)} = -25.2 \pm 5$ mV (mean ± SD, $n = 7$, $P < 0.001$). Steady-state inactivation or s_∞ data were determined from a constant test pulse to 0 mV and plotted as a function of variable conditioning prepulses (duration: 200 ms). Boltzmann fits to individual data sets yielded half-maximal availabilities of channels of $V_{1/2(f)} = -102 \pm 5$ mV (mean ± SD, $n = 5$) and $V_{1/2(s)} = -78 \pm 7$ mV (mean ± SD, $n = 3$) ($P < 6 \times 10^{-05}$). These parameters were used to compute the superimposed fits in the graph (*dotted* and *solid lines*). **C** Unscaled current traces recorded with different pulse protocols from the same patch. *Trace a* was recorded with a holding potential of −100 mV followed by a direct step to 0 mV test potential. In *trace b* the 0 mV test potential was preceded by a 200-ms prepulse to −150 mV

voltage steps showed fast activation followed by a rather slow inactivation over a period of several milliseconds. Subsequent application of the same voltage protocol to the same patch induced Na currents with gradually changing kinetics, yielding apparently accelerated inactivation. In this patch, the transition from slow to fast inactivation gating was virtually complete after 18 min. An increase in maximum peak current could be observed in this and other experiments (four out of ten patches).

Kinetic analysis of Na currents revealed that in all patches examined the inactivation time course was composed of at least two distinguishable components that could be approximated by double-exponential functions with time constants differing about tenfold (e. g. τ_{h1} = approx. 150 μs and τ_{h2} = approx. 2 ms, see also Fig. 4). Kinetic modulation, as shown in Fig. 1 A, involves a relative decrease in A_{h2} normalized to the measured peak current (A_{h2}/I_{max}) for each data trace. Depending on the relative amplitude of A_{h2} and I_{max}, we will refer to Na currents with amplitude ratios A_{h2}/I_{max} of <0.4 and >0.6 as as showing predominantly fast or slow kinetic behavior, respectively. Figure 1 B depicts the time-dependent changes of τ_{h1} and τ_{h2} component amplitudes in four patches. The slow amplitude decreased to about 20% of its original value within 10−30 min (eight out of ten patches), while peak current increased slightly (four out of ten patches) or remained stable. In two patches A_{h2}/I_{max} remained virtually unaltered over time.

The relative proportion of initial fast and slow intercepts could vary between patches. The proportion of patches that started off with predominantly slow kinetics was 70% (seven out of ten patches). Consecutively drawn patches from the same oocyte could have either fast or slow characteristics from the start, with no predictable pattern. However, in no case did we find macroscopic evidence for conversion from fast into slow kinetic behavior.

Slow and fast Na currents differ in voltage sensitivity

We next assessed the $I(V)$ relationships as well as the voltage dependence of activation and steady-state inactivation from Na currents showing predominantly fast or slow gating kinetics. Figure 2 illustrates that channel activation and peak amplitude of slow gating is shifted to more positive potentials by 9 mV as compared to fast gating (Fig. 2 A), whereas neither the reversal potentials for fast and slow kinetics (+45 ± 3.3 mV and +48 ± 2.2 mV) nor the valences (3.2 ± 0.27 and 3.5 ± 0.25) differ significantly (means ± SD, $n = 5$ and 7, respectively). Figure 2 B shows the steady-state activation and inactivation characteristics of fast and slow Na currents. The peak currents have been normalized for maximal conductance and expressed as fraction of open channels $F(V)$. When compared to fast Na currents, half-maximal activation and inactivation of slow currents are shifted to the right along the voltage axis by 10.2 mV and 24 mV, respectively ($n = 5-7$).

Holding potential can be used to select for slow gating channels

The data presented in Fig. 2 B show that the steady-state inactivation (s_∞) curve for fast gating channels lies about

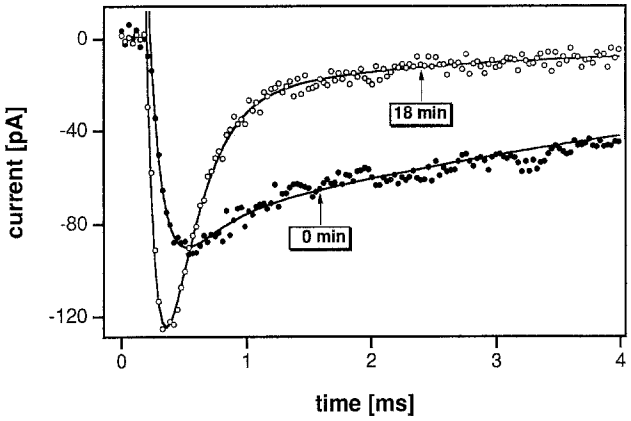

Fig. 3. Concurrent tri-exponential fits to raw data traces at two different times after patch excision. Examples of current records at time zero (●) and 18 min (○) after patch excision. Holding potential was −100 mV, a 200-ms prepulse to −150 mV preceded the test pulse to −10 mV. *Superimposed curves* are tri-exponential fits to the data. For average values of time constants see text

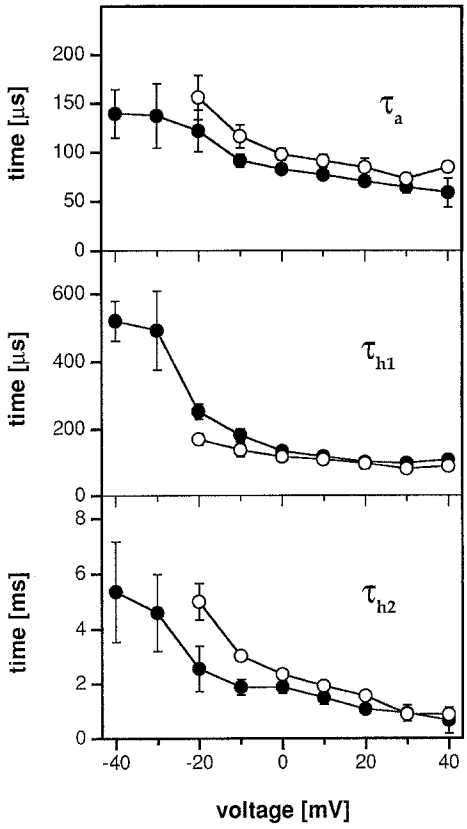

Fig. 4. Voltage dependence of activation and inactivation time constants. Fast mode (●) and slow mode (○) time constant for activation (τ_a) and the two components of inactivation (τ_{h1} and τ_{h2}) are plotted as a function of test potential. Each point represents values of mean time constants ± SEM of fast and slow Na currents (7 and 3 current families, respectively). Note the different time scales of τ_{h1} and τ_{h2}

20 mV to the left of the s_∞ curve for slow gating channels, so that a significant selective suppression of fast gating channels can be expected at holding potentials more positive than about −130 mV. Thus, although we hold excised patches at −100 mV (see Materials and methods) all our protocols were preceded by a 200-ms conditioning pulse to −150 mV, to simulate holding at that potential. In Fig. 2 C we demonstrate the effects of this procedure on the kinetics of test pulse Na currents. Trace *a* shows the current recorded following a direct step from a −100 mV holding potential to a 0 mV test potential. The tri-exponential fitting shows that this current is predominantly slow, with no detectable τ_{h1} kinetics. By contrast, trace *b* shows a current from this same patch obtained following a 200-ms prepulse to −150 mV. This unscaled record shows an almost two-fold larger I_{max} and a marked τ_{h1} component. However, A_{h2} is essentially identical to the I_{max} in trace *a*. Prepulses to potentials between −150 and −100 (data not shown here) demonstrate the progressive suppression of the fast inactivating channels at these intermediate potentials.

This finding clarifies the difference between the fast inactivation kinetics seen in this study and the predominantly slow inactivation rates reported for RB IIA channels expressed in *Xenopus* oocytes by Auld et al. [3, 4] using a holding potential of −100 mV, but without conditioning hyperpolarizing prepulses.

Equilibrium changes between gating modes do not affect time constants

We wondered whether the observed shifts in voltage sensitivity and kinetics could be due to two discrete modal states of Na channels. To this end we performed concurrent tri-exponential analysis of fast and slow current traces to assess the time constants of the rising phase τ_a and the two decaying phases τ_{h1} and τ_{h2} (see Materials and methods).

The traces in Fig. 3 represent currents of the same patch evoked by test pulses to −10 mV, immediately after patch excision and 18 min later. Besides the peak current augmentation and the reduced A_{h2} magnitude of the slow inactivation, no kinetic differences can be detected at this test potential. Time constants as measured in $fast_{(f)}$ or $slow_{(s)}$ currents, did not show statistically significant differences in activation (τ_a) or inactivation (τ_{h1}, τ_{h2}) at −10 mV. For this potential, activation time constants were $\tau_{a(f)} = 103 \pm 17$ µs and $\tau_{a(s)} = 124 \pm 35$ µs (means ± SD, $n = 5$ and 7, respectively). Inactivation time constants for fast currents were $\tau_{h1(f)} = 144 \pm 23$ µs and $\tau_{h2(f)} = 2.1 \pm 1.2$ ms, and for slow currents they were $\tau_{h1(s)} = 134 \pm 39$ µs and $\tau_{h2(s)} = 3.7 \pm 3.2$ ms. To determine whether this result applies to the entire voltage range of inward currents, traces at different test potentials were analyzed. Figure 4 compares the voltage dependence of each time constant for fast and slow gating modes. Overall, comparison of fast and slow gating rates did not reveal significant differences. The apparent difference of the time constant τ_{h2} at test potentials more negative than 0 mV may be due to differences in the $F(V)$ characteristics; at negative potentials slow kinetic amplitudes are less prominent (see Fig. 2 B) and are expected to render larger variations. On the other hand, analysis of a greater number of patches, recorded at

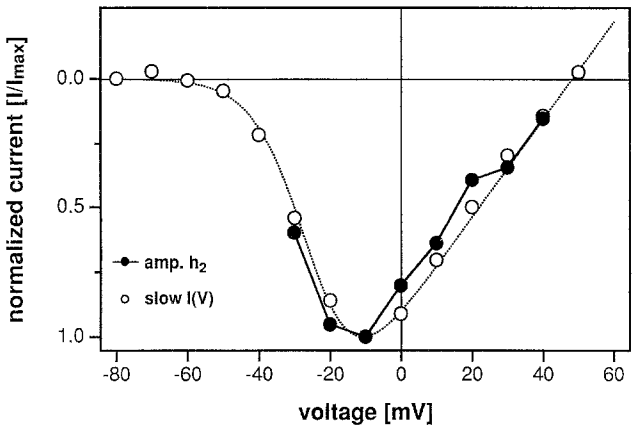

Fig. 5. The $I(V)$ relationship of the slow inactivating component τ_{h2}. Values of A_{h2} (●) as derived from tri-exponential fits (10 current families) and the $I(V)$ relationship of slow mode Na currents (○, identical to the data set in Fig. 2 A) are plotted as a function of test potential. Amplitudes of A_{h2} were normalized to the maximum amplitude (I/I_{max})

higher bandwidths than used in this study, may prove the difference of τ_a between slow and fast gating to be statistically significant at test potentials less than 0 mV. We suspect that currents activate slightly faster in fast mode than in slow mode, although this point cannot yet be substantiated by statistical evaluation.

Amplitudes of slow mode intercepts are voltage dependent

To assess the voltage dependence of the slow gating mode, we determined the A_{h2} values in a total of ten current families (from five patches) that showed a sizeable slow component, regardless of whether the data traces had been classified as fast or slow currents. Within each current family, the amplitudes of A_{h2} at a given potential were normalized to the peak amplitude of A_{h2}. It can be seen that the amplitude of A_{h2} reaches a peak at -10 mV and decreases again (Fig. 5), closely paralleling the $I(V)$ relationship seen for slow Na currents.

Discussion

Macroscopic Na currents in excised patches from *Xenopus* oocytes injected with the α subunit of RBIIA Na channel show time-dependent and unidirectional transitions between at least two gating modes. The $I(V)$ relationship of activation, the fraction of open channels, as well as steady-state inactivation are modified during such transitions. It seems likely that the equilibrium between at least two gating modes of the α subunit determines the phenotype of macroscopic currents, since kinetic analysis does not reveal significant differences between slow and fast inactivation rates. We conclude that the two modes discerned in this study are conferred by two states of Na channels the interconversions of which are regulated by an as yet unknown mechanism that seems to involve cytosolic factors.

Modal gating of Na channels also occurs in native systems such as heart muscle cells [23], frog skeletal muscle [24] or neurons [1, 6]. Distinct gating modes also were reported in *Xenopus* oocyte studies of RBIII or rat skeletal muscle μI channels for whole-oocyte and single-channel recordings [8, 17, 38]. In single-channel cell-attached patch recordings, RBIII channels sometimes switch between the slow and fast mode, whereas μI channels will settle in fast mode regardless of the initial mode after patch formation. It should be pointed out that the terms "fast" and "slow" are used in rather arbitrary ways in different studies. Thus, the time constant for fast inactivation observed in μI single-channel recordings corresponds approximately to the rate we classified as slow mode. However, Zhou et al. [38] mention that the open probability profile of fast gating μI channels revealed an additional, even faster mode which could not be resolved in their ensemble averages, but which could correspond to the phenomenon we term fast mode in this study. Clearly, several kinetic modes with different time scales can be encountered depending on channel type and experimental conditions.

Patch excision seems to influence critically the equilibrium between gating modes of Na channels expressed in *Xenopus* oocytes. In cardiac cells, the slow inactivating component becomes more prominent after patch excision and the channels fluctuate between two major modes [18], quite in contrast to rat brain, where excision tends to speed inactivation [11]. Patch-excision-induced alterations in modal gating indicates the involvement of the cytosolic milieu in controlling mode changes. For example, G proteins have been reported to modulate Na channels [32] and pertussis-toxin-induced reduction of Na currents is counteracted by addition of the human $G_p\alpha_{i-3}$ subunit in the epithelial cell line A6 [5]. Modulatory effects of redox states have been reported for voltage-gated ion channels, affecting inactivation of A-type K channels [29], as well as amplitudes of Ca^{2+}-dependent K currents [26].

Another important regulatory mechanism might be provided by phosphorylation of ion channels. Na channels possess multiple phosphorylation sites for both protein kinase A (PKA) and protein kinase C (PKC). Rapid cyclic-adenosine-monophosphate (cAMP)-dependent protein phosphorylation by PKA reduces ensemble peak Na currents in excised inside-out patches from transfected CHO cells [13]. Moderate activation of PKC by phorbol ester slows Na current inactivation, and stronger activation reduces ensemble peak Na current in RBIIA-transfected CHO cells [22]. Therefore, phosphorylation seems a very plausible candidate for stabilizing distinct gating modes in individual Na channels.

Our results in excised patches – the time-dependent increase in peak current and the modal switch speeding current decay – possibly reflect gradual loss of channel phosphorylation. The degree of phosphorylation may determine the channel's preferential gating behavior, converting consecutively from non-conducting under heavy phosphorylation, to slow mode upon partial dephospho-

rylation, and eventually to preferentially fast mode upon complete dephosphorylation. This hypothesis could explain both our observations of unidirectional mode switching from slow to fast in excised patches and observations of fluctuating mode shifts in cell-attached patches [8, 17, 38], where kinases and phosphatases could regulate the intricate level of modal gating. However, fluctuation of gating modes has also been reported to occur in excised patches [17]. If this phenomenon was also related to phosphorylation-dephosphorylation events, one would have to postulate the presence of parts of the biochemical machinery to sustain channel modulation, even in excised patches. Indications that this might indeed be the case come from enzymatic modulation of muscarinic K channels in excised patches [10]. Our results would then seem compatible with the notion that the preferentially visited gating mode of Na channels is dependent on the incidental presence of specific enzymes in the channel vicinity.

Loss of phosphorylation of specific amino acids could be phosphatase dependent. Evidence for possible involvement of membrane-associated kinases or phosphatases with patchy distribution in the oocyte's membrane is provided by the fact that excised patches from the same oocyte could start off in either fast or slow mode. The fact that some patches started off and remained in slow mode during the recording session would indicate the dependence on phosphatase presence in the excised patch. Phosphatase-independent or use- and voltage-dependent dephosphorylation has not been addressed in our study, but is a speculative possibility. Zhou et al. [38] and Krafte et al. [12] reported speeding of inactivation rates in whole-oocyte currents depending on test pulse frequency.

The perspective of modal gating in Na channels complicates structure-function studies of the protein. Do mutations that shift voltage sensitivity or slow the decay of macroscopic current reflect alterations in the respective functional structures of channel activation and inactivation, or have structures involved in setting the mode of gating been influenced? Further complication arises from the shift in the steady-state inactivation curve, as Na currents will predominantly reflect slow mode characteristics with holding potentials more positive than -100 mV (see Fig. 2 B). This partially explains prior observations of unusually slow inactivation properties of whole-cell Na currents in *Xenopus* oocytes expressing the α subunit [4]. It seems unavoidable that gating modes be considered in structure-function analyses of Na channels, until the underlying mechanism can be experimentally controlled.

Kinetic mode switching may be of importance in developmental processes. The $\beta 1$ subunit normally co-purifies with the α subunit in adult rat brain Na channels [16], but may be expressed differentially at various stages of embryonic development [15]. Co-expression of α and β subunits speeds inactivation and increases peak Na currents [7], while shifting activation and steady-state inactivation to more negative values [25]. Although the mechanism underlying these changes is not known, it appears compatible with switching from slow to fast gating mode. It is conceivable that in native systems the $\beta 1$ subunit, when associated with the α subunit, protects part of the modulation sites which are otherwise exposed to phosphorylation, or other regulatory mechanisms at early stages of development.

Modulation of modal gating of Na channels could have profound physiological implications. Na channels determine the threshold for action potential generation and influence the frequency of neuronal firing in somata and axonal hills. Due to differing voltage sensitivities, the threshold may be determined according to the quantitative distribution of channel gating types. The effect of modal gating may be equally important for the duration of membrane potential changes in cell bodies, which is influenced by Na channel density and open probability. Furthermore, alterations in membrane potential may change Ca^{2+} influx affecting various cellular functions. Variation of Na channel modal gating at such crucial points as synapses could affect regulatory mechanisms of transmitter release.

Acknowledgements. We are grateful to Alan L. Goldin for generously providing the RBIIA cDNA. Our special appreciation goes to John G. Starkus for invaluable support and critical discussions. This study was supported by National Institutes of Health (NIH) Grants no. RO1 NS29204 (to P. C. Ruben) and no. RO1 NS21151 (to J. G. Starkus) as well as grants-in-aid from the American Heart Association (Hawai Affiliate) to J. G. Starkus and P. C. Ruben.

References

1. Alzheimer C, Schwindt PC, Crill WE (1993) Modal gating of Na Channels as a mechanism of persistent Na Current in pyramidal neurons from rat and cat sensorimotor cortex. J Neurosci 13:660–673
2. Armstrong CM, Bezanilla F, Rojas E (1973) Destruction of sodium conductance inactivation in squid axons perfused with pronase. J Gen Physiol 62:375–391
3. Auld VJ, Goldin AL, Krafte DS, Marshall J, Dunn JM, Catterall WA, Lester HA, Davidson N, Dunn RJ (1988) A rat brain Na^+ channel α subunit with novel gating properties. Neuron 1:449–461
4. Auld VJ, Goldin AL, Krafte DS, Catterall WA, Lester HA, Davidson N (1990) A neutral amino acid change in segment IIS4 dramatically alters the gating properties of the voltage-dependent sodium channel. Proc Natl Acad Sci USA 87: 323–327
5. Cantiello HF, Patenause CR, Ausiello DA (1989) G Protein subunit, alpha i-3, activates a pertussis toxin-sensitive Na^+ channel from the epithelial cell line, A6. J. Biol Chem 264:20867–20870
6. Huguenard JR, Hamill OP, Prince DA (1988) Developmental changes in Na^+ conductances in rat neocortical neurons: appearance of a slowly inactivating component. J Neurophysiol 59:778–795
7. Isom LL, De Jongh KS, Reber BFX, Offord J, Charbonneau H, Walsh K, Goldin AL, Catterall WA (1992) Primary structure and functional expression of the $\beta 1$ subunit of the rat brain sodium channel. Science 256:839–842
8. Joho RH, Moormann JR, VanDongen AMJ, Kirsch GE, Silberberg H, Schuster G, Brown AM (1990) Toxin and kinetic profile of rat brain type III sodium channels expressed in *Xenopus* oocytes. Mol Brain Res 7:105–113
9. Kayano T, Noda M, Flockerzi V, Takahashi H, Numa S (1988) Primary structure of rat brain sodium channel III deduced from the cDNA sequence. FEBS Lett 228:187–194

10. Kim D, Lewis DL, Graziadei L, Neer EJ, Bar-Sagi D, Clapham DE (1989) G-protein $\beta\gamma$-subunits activate the cardiac muscarinic K^+ channel via phospholipase A_2. Nature 337: 557–560
11. Kirsch GE, Brown AM (1989) Kinetic properties of single sodium channels in rat heart and rat brain. J Gen Physiol 93:85–99
12. Krafte DS, Goldin AL, Auld VJ, Dunn RJ, Davidson N, Lester HA (1990) Inactivation of cloned Na channels expressed in *Xenopus* oocytes. J Gen Physiol 96:689–706
13. Li M, West JW, Lai Y, Scheuer T, Catterall WA (1992) Functional modulation of brain sodium channels by cAMP-dependent phosphorylation. Neuron 8:1151–1159
14. Loughney K, Kreber R, Ganetzky B (1989) Molecular analysis of the para locus, a sodium channel gene in *Drosophila*. Cell 58:1143–1154
15. McHugh-Sutkowski E, Catterall WA (1990) β1 Subunits of sodium channels. Studies with subunit-specific antibodies. J Biol Chem 265:12393–12399
16. Messner DJ, Catterall WA (1985) The sodium channel from rat brain. Separation and characterization of subunits. J Biol Chem 260:10597–10604
17. Moorman JR, Kirsch GE, VanDongen AMJ, Joho RH, Brown AM (1990) Fast and slow gating of sodium channels encoded by a single mRNA. Neuron 4:243–252
18. Nilius B (1988) Modal gating behavior of cardiac sodium channels in cell-free membrane patches. Biophys J 53:857–862
19. Noda M, Shimizu S, Tanabe T, Takai T, Kayano T, Ikeda T, Takahashi H, Nakayama H, Kanaoka Y, Minamino N, Kangawa K, Matsu H, Raftery M, Hirose S, Inayama H, Hayashida T, Miyata T, Numa S (1984) Primary structure of *Electrophorus electricus* sodium channel deduced from cDNA sequence. Nature 312:121–127
20. Noda M, Ikeda T, Kayano T, Suzuki H, Takashima H, Kurasaki M, Takahashi H, Nakayama H, Numa S (1986) Existence of distinct sodium channel messenger RNAs in rat brain. Nature 320:188–192
21. Noda M, Ikeda T, Kayano T, Suzuki H, Takashima H, Takahashi H, Kuno M, Numa S (1986) Expression of functional sodium channels from cloned cDNA. Nature 322:826–828
22. Numann R, Catterall WA, Scheuer T (1991) Functional modulation of brain sodium channels by protein kinase C phosphorylation. Science 254:115–118
23. Patlak B, Ortiz M (1985) Slow currents through single sodium channels of the adult rat heart. J Gen Physiol 86:89–104
24. Patlak B, Ortiz M (1986) Two modes of gating during late Na^+ channel currents in frog sartorius muscle. J Gen Physiol 87:305–326
25. Patton DE, Isom LL, Catterall WA, Goldin AL (1993) The sodium channel β1 subunit alters gating properties of a variety of sodium channels expressed in *Xenopus* oocytes. Biophys J 64: A5
26. Post JM, Weir K, Archer SL, Hume JR (1993) Redox regulation of K^+ channels and its relationship to hypoxic pulmonary vasoconstriction. Biophys J 64: A227
27. Ramaswami M, Tanouye M (1989) Two sodium-channel genes in *drosophila*: implications for channel diversity. Proc Natl Acad Sci USA 86:2079–2082
28. Rogart RB, Cribbs LL, Muglia LK, Kephart DD, Kaiser MW (1989) Molecular cloning of a putative tetrodotoxin-resistant rat heart Na^+ channel isoform. Proc Natl Acad Sci USA 86:8170–8174
29. Ruppersberg JP, Stocker M, Pongs O, Heinemann S, Frank R, Koenen M (1991) Regulation of fast inactivation of cloned mammalian I_K(A) channels by cysteine oxidation. Nature 352:711–714
30. Salkoff L. Butler A, Wei A, Scavarda N, Giffen K, Ifune C, Goodman R, Mandel G (1987) Genomic organization and deduced amino acid sequence of a putative sodium channel gene in *Drosophila*. Science 237:744–749
31. Scheuer T, Auld VJ, Boyd S, Offord J, Dunn R (1990) Functional properties of rat brain sodium channels expressed in a somatic cell line. Science 247:854–858
32. Schubert B, VanDongen AMJ, Kirsch GE, Brown AM (1989) β-adrenergic inhibition of cardiac sodium channels by dual G-protein pathways. Science 245:516–519
33. Starkus JG, Rayner MD, Fleig A, Ruben PC (1993) Photodynamic modification of sodium channels by methylene blue: effects on fast and slow inactivation. Biophys J 65:715–726
34. Suzuki H, Beckh S, Kubo H, Yahagi N, Ishida H, Kayano T, Noda M, Numa S (1988) Functional expression of cloned cDNA encoding sodium channel III. FEBS Lett 228:195–200
35. Trimmer JS, Cooperman SS, Tomiko SA, Zhou J, Crean SM, Boyle MB, Kallen RG, Sheng Z, Barchi RL, Sigworth FJ, Goodman RH, Agnew WS, Mandel G (1989) Primary structure and functional expression of a mammalian skeletal muscle sodium channel. Neuron 3:33–49
36. Vassilev PM, Scheuer T, Catterall WA (1989) Identification of an intracellular peptide segment in sodium channel inactivation. Science 241:1658–1661
37. West JW, Scheuer T, Maechler L, Catterall WA (1992) Efficient expression of rat brain type IIA Na^+ channel α subunits in a somatic cell line. Neuron 8:59–70
38. Zhou J, Potts JF, Trimmer JS, Agnew WS, Sigworth FJ (1991) Multiple gating modes and the effect of modulating factors on the μI sodium channel. Neuron 7:775–785